Chapter 4
Casimir Effect in the Scattering Approach: Correlations Between Material Properties, Temperature and Geometry

Astrid Lambrecht, Antoine Canaguier-Durand, Romain Guérout and Serge Reynaud

Abstract We present calculations of the quantum and thermal Casimir interaction between real mirrors in electromagnetic fields using the scattering approach. We begin with a pedagogical introduction of this approach in simple cases where the scattering is specular. We then discuss the more general case of stationary arbitrarily shaped mirrors and present in particular applications to two geometries of interest for experiments, that is corrugated plates and the plane-sphere geometry. The results nicely illustrate the rich correlations existing between material properties, temperature and geometry in the Casimir effect.

4.1 Introduction

The Casimir effect [1] is an observable effect of vacuum fluctuations in the mesoscopic world, to be tested with the greatest care as a crucial prediction of quantum field theory [2–8]. It also constitutes a fascinating interface between quantum field theory and other important aspects of fundamental physics, for example through its connection with the problem of vacuum energy [9–11].

A. Lambrecht (✉) · A. Canaguier-Durand · R. Guérout · S. Reynaud
Laboratoire Kastler Brossel, CNRS, ENS, Université Pierre et Marie Curie case 74,
Campus Jussieu, 75252 Paris Cedex 05, France
e-mail: astrid.lambrecht@upmc.fr

A. Canaguier-Durand
e-mail: antoine.canaguier@upmc.fr

R. Guérout
e-mail: romain.guerout@upmc.fr

S. Reynaud
e-mail: serge.reynaud@upmc.fr

Casimir physics plays an important role in the tests of gravity at sub-millimeter ranges [12, 13]. Strong constraints have been obtained in short range Cavendish-like experiments [14]. A hypothetical new force of Yukawa-like form could not exceed the gravitational force in the range above 56 μm. For ranges of the order of the micrometer, similar tests are performed by comparing the results of Casimir force measurements with theoretical predictions [15–17]. At even shorter scales, those tests can be performed using atomic [18] or nuclear [19] force measurements. In any of these short-range gravity tests, a new hypothetical force would appear as a difference between the experimental result F_{exp} and the theoretical prediction F_{th}. This implies that F_{th} and F_{exp} have to be assessed independently from each other and necessarily forbids use of the theory-experiment comparison for proving (or disproving) some specific experimental result or theoretical model.

Finally, the Casimir force and the closely related Van der Waals force are dominant at micron or sub-micron distances, entailing their strong connections with various important domains, such as atomic and molecular physics, condensed matter and surface physics, chemical and biological physics, micro- and nano-technology [20].

4.2 Comparison of Casimir Force Measurements with Theory

Casimir calculated the force between a pair of perfectly smooth, flat and parallel plates in the limit of zero temperature and perfect reflection which led him to the universal expressions for the force F_{Cas} and energy E_{Cas}

$$F_{Cas} = -\frac{\hbar c \pi^2 A}{240 L^4}, \quad E_{Cas} = -\frac{\hbar c \pi^2 A}{720 L^3}. \tag{4.1}$$

with L the mirrors' separation, A their surface, c the speed of light and $\hbar$ the Planck constant. The universality of these ideal Casimir formulas is explained by the saturation of the optical response of perfect mirrors which exactly reflect 100% of the incoming fields. This idealization does not correspond to any real mirror. In fact, the effect of imperfect reflection is large in most experiments, and a precise knowledge of its frequency dependence is essential for obtaining reliable theoretical predictions to be compared with Casimir force measurements [21–35]. See also the chapter of van Zwol et al. in this volume for additional discussions of characterization of optical properties in Casimir force experiments.

4.2.1 The Description of Metallic Mirrors

The most precise experiments are performed with metallic mirrors which are good reflectors at frequencies smaller than their plasma frequency ω_P. Their optical response at a frequency ω is described by a reduced dielectric function written as

$$\varepsilon[\omega] = \bar{\varepsilon}[\omega] + \frac{\sigma[\omega]}{-i\omega}, \quad \sigma[\omega] = \frac{\omega_{\mathrm{P}}^2}{\gamma - i\omega}. \tag{4.2}$$

The function $\bar{\varepsilon}[\omega]$ represents the contribution of interband transitions and it is regular at the limit $\omega \to 0$. Meanwhile $\sigma[\omega]$ is the reduced conductivity, measured as a frequency (the SI conductivity is $\epsilon_0 \sigma$,) which describes the contribution of the conduction electrons.

A simplified description corresponds to the lossless limit $\gamma \to 0$ often called the plasma model. As γ is much smaller than ω_{P} for good conductors, this simple model captures the main effect of imperfect reflection. However it cannot be considered as an accurate description since a much better fit of tabulated optical data is obtained with a non null value of γ [36, 37]. Furthermore, the Drude model, with $\gamma \neq 0$, meets the important property of ordinary metals which have a finite static conductivity $\sigma_0 = \frac{\omega_{\mathrm{P}}^2}{\gamma}$, in contrast to the lossless limit which corresponds to an infinite value for σ_0.

Another correction to the Casimir expressions is associated with the effect of thermal fluctuations [38–41]. Boström and Sernelius have remarked that the small non zero value of γ had a significant effect on the force evaluation at ambient temperature [42]. This significant difference is attributed to the vanishing contribution of TE modes at zero frequency for dissipative mirrors entailing that for the Casimir force, contrary to the dielectric function, there is no continuity from the Drude to the plasma model at the limit of a vanishing relaxation. The ratio between the predictions evaluated at $\gamma = 0$ and $\gamma \neq 0$ even reaches a factor of 2 at the limit of large temperatures or large distances. Unfortunately it has not yet been possible to test this striking prediction since the current experiments do not explore this domain.

The current status of Casimir experiments appears to favor theoretical predictions obtained with the lossless plasma model $\gamma = 0$ rather than those corresponding to the Drude model with $\gamma \neq 0$ as one might have expected (see Fig. 4.1 in [29]). See the chapter by Decca et al. in this volume for additional discussions of this observation. We thus have to face a discrepancy between theory and experiment. This discrepancy may have various origins, in particular artifacts in the experiments or inaccuracies in the calculations. They may also come from yet unmastered differences between the situations studied in theory and the experimental realizations.

These remarks have led to a blossoming of papers devoted to the thermal effect on the Casimir force, for reviews see e.g. [43–47]. It is worth emphasizing that microscopic descriptions of the Casimir interaction between two metallic bulks lead to predictions agreeing with the lossy Drude model rather than the lossless plasma model at the limit of large temperatures or large distances [48–50].

It is also important to note that the Drude model leads to a negative contribution of the Casimir interaction to entropy, in contrast to the plasma model [51]. There is no principle inconsistency with the laws of thermodynamics at this point since the negative contribution is nothing but a difference of entropies (see for example [52]).

Fig. 4.1 Two plane parallel
plates at distance L facing
each other constitute the
Casimir cavity

$$A \gg L^2$$

$$L$$
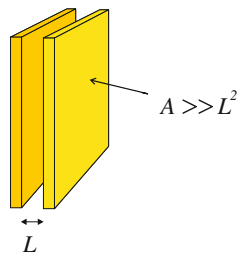
4.2.2 The Role of Geometry

The geometry plays an important role in the context of theory/experiment comparison for Casimir forces. Precise experiments are indeed performed between a plane and a sphere whereas most exact calculations are devoted to the geometry of two parallel plates. The estimation of the force in the plane-sphere geometry thus involves the so-called *Proximity Force Approximation* (PFA) [53] which amounts to averaging the force calculated in the parallel-plates geometry over the distribution of local inter-plate distances, the force being deduced from the Lifshitz formula [54, 55], the meaning of which will be discussed below.

This trivial treatment of geometry cannot reproduce the rich interconnection expected to take place between the Casimir effect and geometry [56–59]. In the plane-sphere geometry in particular, the PFA can only be valid when the radius R is much larger than the separation L [60–62]. But even if this limit is met in experiments, the PFA gives no information about its accuracy for a given ratio of L/R and how this accuracy depends on the properties of the mirror, on the distance or temperature.

Answers to these questions can only be obtained by pushing the theory beyond the PFA, which has been done in the past few years [63–67]. A multipolar expansion of the Casimir effect between perfect mirrors in electromagnetic vacuum was proposed in [68, 69]. These calculations have now been performed for plane and spherical metallic surfaces coupled to electromagnetic vacuum, at zero [70] or non zero temperature [71, 72], which has opened the way to a comparison with theory of the only experimental study devoted to a test of PFA in the plane-sphere geometry [73]. As we will see at the end of this article, the features of the thermal Casimir force mentioned in Sect. 4.2 are considerably altered when the geometry is properly taken into account. The factor of 2 between the force values within Drude and plasma model is reduced to a factor of 3/2, decreasing even more below this value when small spheres are considered. Negative entropies are not only found for the Drude model but also for perfect reflector and plasma models, which means that negative contributions of the Casimir interaction to entropy can be found even in the absence of dissipation.

Another specific geometry of great interest, that we will present in the following, is that of surfaces with periodic corrugations. As lateral translation symmetry is broken, the Casimir force contains a lateral component which is smaller

than the normal one, but has nevertheless been measured in dedicated experiments [74, 75]. Calculations beyond the PFA were first performed with the simplifying assumptions of perfect reflection [76] or shallow corrugations [77–79]. As expected, the PFA was found to be accurate only in the limit of large corrugation wavelengths. Very recently, experiments have been able to probe the beyond-PFA regime [80, 81] and exact calculations of the forces between real mirrors with deep corrugations [82, 83] have been performed. More discussions on these topics will be presented below.

4.3 The Scattering Approach

In the following, we will focus our attention on the scattering approach, which is an efficient and elegant method for addressing the aforementioned questions.

This method has been used for years for describing the optical properties of non-perfectly reflecting mirrors in terms of scattering amplitudes [84, 85]. These scattering amplitudes are often deduced from Fresnel reflection amplitudes calculated for mirrors described by local dielectric response functions, in which case the expression of the Casimir force is reduced to the Lifshitz expression [54, 55]. However the scattering approach is much more general than the Lifshitz one since real mirrors are always described by some scattering amplitudes but not necessarily by local dielectric response functions. This point will be discussed in more detail below.

The interest in the scattering approach has considerably increased since it has become clear that it is also an extremely efficient method for calculating the Casimir effect in non-trivial geometries. This was realized by several groups employing different theoretical techniques and using different notations (see [86] for an historial overview). Besides the already quoted papers, one may cite the following references which used different versions of the scattering approach [64, 87–92] or alternative methods [93–98]. This topic has seen recently an impressive number of new applications proposed, among which one may cite [99–106]. See also the chapter of Rahi et al. in this volume for additional discussions of the scattering approach in Casimir physics.

An early application of the scattering approach to non-trivial geometries and non-perfect reflectors was developed in [107, 108] to calculate the roughness correction to the Casimir force between two planes, in a perturbative expansion with respect to the roughness amplitude. The same perturbative formalism was also applied to compute the lateral Casimir force [77–79] and the Casimir torque [109] between two corrugated surfaces made of real material, and then to derive the Casimir-Polder potential for an atom near a corrugated surface [111, 112].

Let us recall that results applicable to the non-retarded case have been available [113, 114] before those corresponding to the full retarded theory, and also that the scattering theory has been used for a long time for studying the Casimir-Polder force between atoms and molecules [115, 116].

We begin the review of the scattering approach by an introduction considering the two simple cases of the Casimir force between two scatterers on a 1-dimensional line and between two parallel plates coupled through specular scattering to 3-dimensional electromagnetic fields [84]. We then address the general case of non-specular scatterers in 3-dimensional electromagnetic fields [8].

4.3.1 Mirrors on a 1-Dimensional Line

The first case corresponds to the quantum field theory in 2-dimensional spacetime (1-d space plus time). In this simple case, we have to consider only two scalar fields counter-propagating along opposite directions. The results summarized below are drawn from a series of papers devoted to the study of static or dynamic Casimir force between mirrors coupled to these scalar fields [9, 84, 117–125]. For example, it was established in [118] that the Casimir energy does contribute to the inertia of the cavity as it should according to the principles of relativity.

In this simple model, a mirror M_1 at rest at position q_1 is described by a 2×2 scattering matrix S_1 containing reflection and transmission amplitudes r_1 and t_1

$$S_1 = \begin{bmatrix} t_1 & r_1 e^{-2i\omega q_1/c} \\ r_1 e^{2i\omega q_1/c} & t_1 \end{bmatrix}. \tag{4.3}$$

Two mirrors M_1 and M_2 at rest at positions q_1 and q_2 form a Fabry–Perot cavity described by a global scattering matrix S_{12} which can be deduced from the elementary matrices S_1 and S_2 associated with the two mirrors.

$$S_{12} = \frac{1}{d} \begin{bmatrix} t_1 t_2 & dr_2 e^{-i\omega L/c} + t_2^2 r_1 e^{i\omega L/c} \\ dr_1 e^{-i\omega L/c} + t_1^2 r_2 e^{i\omega L/c} & t_1 t_2 \end{bmatrix}. \tag{4.4}$$

The denominator d is given by

$$d = 1 - r_1 r_2 e^{2i\omega L/c}, \quad L \equiv q_2 - q_1, \tag{4.5}$$

and its zeros (the poles of S_{12}) represent the resonances of the cavity. It turns out that the forthcoming discussion of the Casimir effect depend only on the expression of d and not on all the other details in the form of S_{12}. The reason explaining this property is the following relation between the determinants of the S–matrices (all supposed to be unitary in the simple model):

$$\det S_{12} = (\det S_1)(\det S_2)\left(\frac{d^*}{d}\right). \tag{4.6}$$

From this relation, it is easy to derive the Casimir free energy as a variation of field energy (vacuum energy at $T = 0$, vacuum plus thermal energy otherwise). The presence of a scatterer indeed shifts the field modes and thus induces a variation of the global field energy. The Casimir free energy is then obtained as the variation of

field energy in presence of the cavity corrected by the effects of each mirror taken separately [84]

$$\mathcal{F} \equiv \delta\mathcal{F}_{\text{field},12} - \delta\mathcal{F}_{\text{field},1} - \delta\mathcal{F}_{\text{field},2} = -\int_0^\infty \frac{d\omega}{2\pi} N\hbar\Delta. \qquad (4.7)$$

Δ is a function of the frequency ω representing the phase-shift produced by the Fabry–Perot cavity, again corrected by the effects of each mirror taken separately

$$\Delta(\omega) = \frac{\ln \det S_{12} - \ln \det S_1 - \ln \det S_2}{i} = \frac{1}{i}\ln\left(\frac{d^*}{d}\right). \qquad (4.8)$$

N is the mean number of thermal photons per mode, given by the Planck law, augmented by the term $\frac{1}{2}$ which represents the contribution of the vacuum

$$N(\omega) = \frac{1}{2} + \frac{1}{\exp\frac{\hbar\omega}{k_{\text{B}}T} - 1} = \frac{1}{2\tanh\frac{\hbar\omega}{2k_{\text{B}}T}}. \qquad (4.9)$$

This phase-shift formula can be given alternative interpretations [84]. In particular, when the Casimir force F is derived from the free energy

$$F = -\frac{\partial\mathcal{F}(L,T)}{\partial L} = \int_0^\infty \frac{d\omega}{\pi}\frac{N\hbar\omega}{c}(f + f^*) = \int_0^\infty \frac{d\omega}{\pi}\frac{N\hbar\omega}{c}(g - 1),$$

$$f \equiv \frac{re^{2i\omega L/c}}{1 - re^{2i\omega L/c}}, \quad g \equiv \frac{1 - \left|re^{2i\omega L/c}\right|^2}{\left|1 - re^{2i\omega L/c}\right|^2}, \qquad (4.10)$$

it is seen as resulting from the difference of radiation pressures exerted onto the inner and outer sides of the mirrors by the field fluctuations. For each field mode at frequency ω, $\frac{N\hbar\omega}{c}$ represents the field momentum while g is the ratio of fluctuation energies inside and outside the Fabry–Perot cavity.

Using the analytic properties of the causal function $\ln d$, the Casimir free energy can also be written as an integral over imaginary frequencies $\omega = i\xi$ (Wick rotation)

$$\mathcal{F} = \hbar \int \frac{d\xi}{2\pi}\cot\left(\frac{\hbar\xi}{2k_{\text{B}}T}\right)\ln d(i\xi). \qquad (4.11)$$

Using the pole decomposition of the cotangent function and the analytic properties of $\ln d$, this expression can finally be written as a sum over Matsubara frequencies

$$\mathcal{F} = k_{\text{B}}T \sum_m{}' \ln d(i\xi_m), \quad \xi_m \equiv \frac{2\pi m k_{\text{B}}T}{\hbar}. \qquad (4.12)$$

The Matsubara sum $\sum_m'$ is the sum over positive integers m with $m = 0$ counted with a weight $\frac{1}{2}$.

For completeness, let us recall also that the contribution to entropy of the Casimir interaction is simply written as

$$S \equiv -\frac{\partial \mathcal{F}(L, T)}{\partial T}. \tag{4.13}$$

Hence, it is defined as a difference of entropies just as the free energy $\mathcal{F}$ has been defined in (4.7) above as a difference of free energies.

4.3.2 Specular Reflection in 3-d Space

The same lines of reasoning can be followed when studying the case of two specularly reflecting mirrors coupled to electromagnetic fields in 3-dimensional space. The geometry is sketched in Fig. 4.1 with two plane parallel mirrors aligned along the transverse directions x and y (longitudinal direction denoted by z).

Due to the symmetry of this configuration, the frequency ω, the transverse vector $\mathbf{k} \equiv (k_x, k_y)$ and the polarization $p = \mathrm{TE}, \mathrm{TM}$ are preserved by all scattering processes. The mirrors are described by reflection and transmission amplitudes which depend on these scattering parameters. We assume thermal equilibrium for the whole "cavity + fields" system, and proceed with the derivation as in the simpler case of a 1-dimensional space. Some elements have to be treated with greater care now [85, 8]. First there is a contribution of evanescent waves besides that of ordinary modes freely propagating outside and inside the cavity and it has to be taken carefully into account. The properties of the evanescent waves are described through an analytical continuation of those of ordinary ones, using the well defined analytic behavior of the scattering amplitudes. Then dissipation inside the mirrors may also play a role which implies considering the additional fluctuation lines coming along with dissipation [8, 85].

At the end of this derivation the free energy may still be written as a Matsubara sum

$$\mathcal{F} = k_{\mathrm{B}}T \sum_{\mathbf{k}} \sum_{p} \sum_{m}' \ln d(i\xi_m, \mathbf{k}, p), \quad \xi_m \equiv \frac{2\pi m k_{\mathrm{B}}T}{\hbar},$$

$$\sum_{\mathbf{k}} \equiv A \int \frac{\mathrm{d}^2 \mathbf{k}}{4\pi^2} \equiv A \int \frac{\mathrm{d}k_x \mathrm{d}k_y}{4\pi^2}. \tag{4.14}$$

$\sum_{\mathbf{k}}$ is the sum over transverse wavevectors with A the area of the plates, $\sum_{p}$ the sum over polarizations and $\sum_{m}'$ the same Matsubara sum as in the 1-d case. The denominator is now written in terms of the result κ of Wick rotation on the longitudinal wavevector k_z

$$d(i\xi, \mathbf{k}, p) = 1 - r_1(i\xi, \mathbf{k}, p) r_2(i\xi, \mathbf{k}, p) \exp^{-2\kappa L},$$

$$\kappa \equiv \sqrt{\mathbf{k}^2 + \frac{\xi^2}{c^2}}. \tag{4.15}$$

This expression reproduces the ideal Casimir formula (4.1) in the limits of perfect reflection $r_1 r_2 \to 1$ and zero temperature $T \to 0$. It is valid and regular at thermal equilibrium at any temperature and for any optical model of mirrors obeying causality and high frequency transparency properties [8, 84, 85]. It can thus be used for calculating the Casimir force between arbitrary mirrors, as soon as the reflection amplitudes are specified. These amplitudes are commonly deduced from models of mirrors, the simplest of which is the well known Lifshitz model [54, 55] which corresponds to semi-infinite bulk mirrors characterized by a local dielectric response function $\varepsilon(\omega)$ and reflection amplitudes deduced from the Fresnel law

$$r_{\text{TE}}(\mathbf{k}, \xi) = \frac{\kappa - \kappa_t}{\kappa + \kappa_t}, \quad r_{\text{TM}}(\mathbf{k}, \xi) = \frac{\varepsilon \kappa - \kappa_t}{\varepsilon \kappa + \kappa_t}, \tag{4.16}$$

$$\kappa_t \equiv \sqrt{\mathbf{k}^2 + \varepsilon \frac{\xi^2}{c^2}}. \tag{4.17}$$

ε is the dielectric function (4.2) and κ_t denotes the result of Wick rotation of the longitudinal wavevector inside the medium.

In the most general case, the optical response of the mirrors cannot be described by a local dielectric response function. The expression (4.14) of the free energy is still valid in this case with the reflection amplitudes to be determined from microscopic models of mirrors. Recent attempts in this direction can be found for example in [126–133].

At this stage, several remarks can be addressed to the readers interested in historical details:

- The Lifshitz expression was not written in terms of reflection amplitudes until Kats noticed that this formulation was natural [134]. To our best knowledge, the first appearance of an expression of the Casimir effect in terms of reflection amplitudes corresponding to an arbitrary microscopic model (not necessarily a dielectric response function) is in [84].
- The fact that the expression (4.14) of the free energy is valid for lossy as well as lossless mirrors is far from obvious. In the lossy case, one has indeed to take into account the contributions of fluctuations coming from the additional modes associated with dissipation. This property has been demonstrated with an increasing range of validity in [84, 85] and [8] (see also [135] for a theorem playing a crucial role in this demonstration).
- The question had been asked in [43] whether the regularity conditions needed to write the Matsubara sum were met for the Drude model which shows discontinuities at $\xi \to 0$. This question has been answered positively in [52].

4.3.3 The Non-specular Scattering Formula

We now present a more general scattering formula allowing one to calculate the Casimir force between stationary objects with arbitrary shapes. We restrict our attention to the case of disjoint objects, exterior to each other, which corresponds to the configuration initially considered by Casimir (for interior configurations, which may be treated with similar techniques, see for example [136–139]).

The main generalization with respect to the already discussed specular cases is that the scattering matrix $\mathbb{S}$ has now to account for non-specular reflection. It is therefore a much larger matrix which mixes different wavevectors and polarizations while preserving frequency as long as the scatterers are stationary [8]. Of course, the non-specular scattering formula is the generic one while specular reflection can only be an idealization.

As previously, the Casimir free energy can be written as the sum of all the phase-shifts contained in the scattering matrix

$$\mathcal{F} = i\hbar \int\limits_0^\infty \frac{\mathrm{d}\omega}{2\pi} N(\omega) \ln \det \mathbb{S} = i\hbar \int\limits_0^\infty \frac{\mathrm{d}\omega}{2\pi} N(\omega) \mathrm{Tr} \ln \mathbb{S}. \qquad (4.18)$$

The symbols det and Tr refer to determinant and trace over the modes of the scattering matrix at a given frequency ω. After a Wick rotation the formula can still be written as a Matsubara sum

$$\mathcal{F} = k_\mathrm{B}T \sum_m {}' \mathrm{Tr} \ln D(i\xi_m), \quad \xi_m \equiv \frac{2\pi m k_\mathrm{B}T}{\hbar}. \qquad (4.19)$$

The matrix D (here written at Matsubara frequencies $\omega_m = i\xi_m$) is the denominator of the scattering matrix. It describes the resonance properties of the cavity formed by the two objects 1 and 2 and may be written as

$$D = 1 - R_1 \exp^{-KL} R_2 \exp^{-KL}. \qquad (4.20)$$

The matrices R_1 and R_2 represent reflection on the two objects 1 and 2 respectively while $\exp^{-KL}$ describes propagation in between reflections on the two objects. Note that the matrices D, R_1 and R_2, which were diagonal in the plane wave basis for specular scattering, are no longer diagonal in the general case of non-specular scattering. The propagation factors remain diagonal in this basis with their eigenvalues κ written as in (4.14). Clearly the expression (4.19) does not depend on the choice of a specific basis. We remark also that (4.19) takes a simpler form in the limit of zero temperature

$$F = -\frac{\mathrm{d}E}{\mathrm{d}L}, \quad E = \hbar \int\limits_0^\infty \frac{\mathrm{d}\xi}{2\pi} \ln \det D(i\xi). \qquad (4.21)$$

Applications to be presented in the next sections will also involve the Casimir force gradient G which is often measured in experiments and defined as

$$G = -\frac{\mathrm{d}F}{\mathrm{d}L}. \tag{4.22}$$

A number of the following applications will be discussed within the zero temperature limit, with a change of notation from the free energy $\mathcal{F}$ to the ordinary energy E at zero temperature.

4.4 Applications to Non-trivial Geometries

Formula (4.21) has been used to evaluate the effect of roughness or corrugation of the surfaces on the value of the Casimir force [107, 77–79, 31] in a perturbative manner with respect to the roughness or corrugation amplitudes. It has also allowed one to study a Bose–Einstein condensate used as a local probe of vacuum above a nano-grooved plate [111, 112]. The scattering approach has clearly a larger domain of applicability, not limited to the perturbative regime, as soon as techniques are available for computing the large matrices involved in its evaluation [82, 83, 140].

Another important application, which we will summarize also in the present section, corresponds to the plane-sphere geometry used in most Casimir force experiments and for which explicit "exact calculations" (see a discussion of the meaning of this expression below) have recently become available [68–72].

4.4.1 Perturbative Treatment of Shallow Corrugations

As already stated, the lateral Casimir force between corrugated plates is a topic of particular interest. It could in particular allow for a new test of quantum electrodynamics through the dependence of the lateral force on the corrugation wavevector [77–79].

Here, we consider a geometry with two plane mirrors, M_1 and M_2, having corrugated surfaces described by uniaxial sinusoidal profiles such as shown in Fig. 4.2. We denote h_1 and h_2 the local heights with respect to mean planes $z_1 = 0$ and $z_2 = L$

$$h_1 = a_1 \cos(k_C x), \quad h_2 = a_2 \cos(k_C(x - b)), \quad k_C = 2\pi/\lambda_C. \tag{4.23}$$

h_1 and h_2 have null spatial averages and L is the mean distance between the two surfaces; h_1 and h_2 are both counted as positive when they correspond to a decrease in the separation; λ_C is the corrugation wavelength, k_C the corresponding wavevector, and b the spatial mismatch between the corrugation crests. At lowest
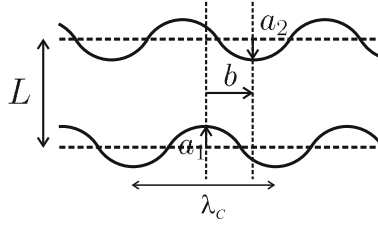
Fig. 4.2 Parallel corrugated surfaces, with L representing the mean separation distance, a_1 and a_2 the corrugation amplitudes and b the lateral mismatch between the crests. When the corrugations are supposed to be the smallest length scales, the effect of the corrugations can be studied in the perturbative expansion. This approximation will be dropped later on

order in the corrugation amplitudes, when $a_1, a_2 \ll \lambda_C, \lambda_P, L$ (with λ_P the plasma wavelength describing the properties of the metallic mirror), the Casimir energy may be obtained by expanding up to second order the general formula (4.21). This perturbative approximation will be dropped in the next subsection.

The part of the Casimir energy able to produce a lateral force is then found to be

$$
\begin{aligned}
F^{\text{lat}} &= -\frac{\partial \delta E^{\text{corrug}}}{\partial b}, \\
\delta E^{\text{corrug}} &= -\hbar \int\limits_{0}^{\infty} \frac{d\xi}{2\pi} \text{Tr}\left(\delta R_1 \frac{\exp^{-KL}}{D_{\text{plane}}} \delta R_2 \frac{\exp^{-KL}}{D_{\text{plane}}} \right).
\end{aligned}
\tag{4.24}
$$

δR_1 and δR_2 are the first-order variation of the reflection matrices R_1 and R_2 induced by the corrugations; D_{plane} is the matrix D evaluated at zeroth order in the corrugations; it is diagonal on the basis of plane waves and commutes with K.

Explicit calculations of (4.24) have been performed for the simplest case of experimental interest, with two corrugated metallic plates described by the plasma dielectric function. These calculations have led to the following expression of the lateral part of the Casimir energy

$$
\delta E^{\text{corrug}} = \frac{A}{2} G_{\text{C}}(k_{\text{C}}) a_1 a_2 \cos(k_{\text{C}} b).
\tag{4.25}
$$

The spectral sensitivity function $G_{\text{C}}(k_{\text{C}})$ has been given and discussed in [79]. Using its expression, it is possible to prove a properly defined "Proximity Force Theorem" which states that the PFA is recovered at the limit of long corrugation wavelengths $k_{\text{C}} \to 0$. Obviously, this theorem does not imply that the PFA is always valid or, in other words, that $G_{\text{C}}(k_{\text{C}})$ may be replaced by $G_{\text{C}}(0)$.

To assess the validity of the PFA for the lateral Casimir force description, we now introduce the dimensionless quantity

$$
\rho(k_{\text{C}}) = \frac{G_{\text{C}}(k_{\text{C}})}{G_{\text{C}}(0)}.
\tag{4.26}
$$

Fig. 4.3 Variation of ρ versus the dimensionless variable $k_C L$ for metallic mirrors described by the plasma model, for $k_P L = 1$ (*dashed line*), 2.5 (*dotted line*), 5 (*dashed-dotted line*) and 10 (*solid line*)
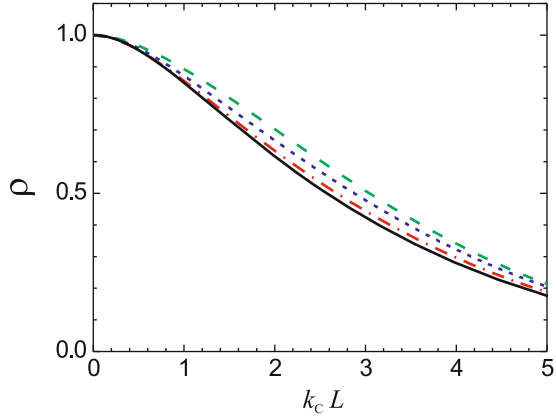
The variation of this ratio ρ with the parameters of interest is shown in Fig. 4.3 for gold covered plates with $\lambda_P = 137$ nm. The ratio ρ is smaller than unity as soon as k_C significantly deviates from 0 which means that the PFA overestimates the lateral Casimir force. For large values of k_C, it even decays exponentially to zero, leading to an extreme deviation of the real lateral force from the PFA prediction.

Another situation of interest arises when the corrugation plates are rotated with respect to each other. Assuming as previously corrugations of sinusoidal shape with corrugation wavevectors $\mathbf{k}_j$ having the same modulus $k = 2\pi/\lambda_C$ on both plates, it is possible to derive the second-order correction δE^{torque} to the Casimir energy which depends on the angle θ between the corrugations and thus has the ability to induce a Casimir torque [77, 78, 109]. Only crossed terms, proportional to the corrugation amplitudes on both plates, contribute to this expression, as the square terms are independent of the angle θ. The expression δE^{torque} contains as the special case $\theta = 0$ the pure lateral energy discussed above. Note that the dependence on the material properties and corrugation wavevector are captured by the same response function G_C already calculated.

For quantitative estimations, we assume that the corrugations are restricted to a rectangular section of area $L_x L_y$ with transverse dimensions L_x and L_y much larger than the plate separation L and neglect diffraction at the borders of the plates. In Fig. 4.4, we plot δE^{torque} obtained in this manner, in arbitrary units, as a function of b and θ. The Casimir energy is found to be minimal at $\theta = 0$ and $b = 0, \lambda_C, 2\lambda_C, \ldots$, which corresponds to a situation where corrugations are aligned. Starting from $\theta = b = 0$ and rotating plate 2 around its center, one follows the line $b = 0$ in Fig. 4.4. Clearly, for small angles the plate is attracted back to $\theta = b = 0$ without sliding laterally.

The Casimir torque is then deduced by deriving the energy with respect to the angle θ

$$\tau = -\frac{\partial}{\partial \theta} \delta E^{\text{torque}}. \tag{4.27}$$

Fig. 4.4 Casimir energy as a
function of the rotation angle θ
and the lateral displacement b
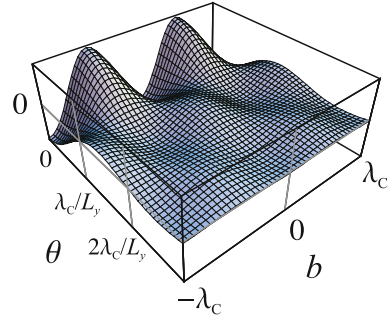
Its maximum is at $\theta = 0.66\lambda_C/L_y$ where it is given by

$$\frac{\tau}{L_x L_y} = 0.109 a_1 a_2 k G_C(k) L_y. \tag{4.28}$$

The maximum torque per unit area is proportional to the length L_y of the corrugation lines, which plays the role of the moment arm.

In contrast with the similar torque appearing between misaligned birefringent plates [141], the torque is here coupled to the lateral force. This could induce complicated behaviors in an experiment and would probably have to be controlled. This can be clearly seen on Fig. 4.4: if the plate is released after a rotation of $\theta > \lambda_C/L_y$ it will move in a combination of rotation and lateral displacement. The energy correction vanishes at $\theta = \lambda_C/L_y$, defining the range of stability of the configuration $b = \theta = 0$. Rotation is favored over lateral displacements only for $\theta < \lambda_C/L_y$.

However, the advantage of the configuration with corrugated plates is that the torque has a larger magnitude. Fig. 4.5 shows the maximum torque as a function of mean separation between the two corrugated gold plates with a plasma wavelength $\lambda_P = 137$ nm. At a plate separation of about 100 nm the torque per unit area can be as high as 10^{-7} N m^{-1} These results on lateral forces and Casimir torques suggest that non-trivial effects of geometry, i.e. effects beyond the PFA, can be observed with dedicated experiments. It is however difficult to achieve this goal with corrugation amplitudes a_1, a_2 meeting the conditions of validity of the perturbative expansion. This approximation is dropped in the next subsection.

4.4.2 Non-perturbative Calculations with Deep Gratings

As already stated, recent experiments have been able to probe the beyond-PFA regime with deep corrugations [80, 81] and it has also become possible to calculate exact expressions of the forces between nanostructures without using the perturbative assumption. This necessarily involves the non-specular scattering formula

Fig. 4.5 Maximum torque per unit area as a function of the mean separation L for the following parameters: $a_1 a_2 = 200\,\text{nm}^2$, $L_y = 24\,\mu\text{m}$, $\lambda_P = 137\,\text{nm}$. *Solid line*: $\lambda_C = 2.4\,\mu\text{m}$; *dashed line*: $\lambda_C = 1.2\,\mu\text{m}$; *dotted line*: $\lambda_C = 2\pi L/2.6$ (corresponding to the optimum value)
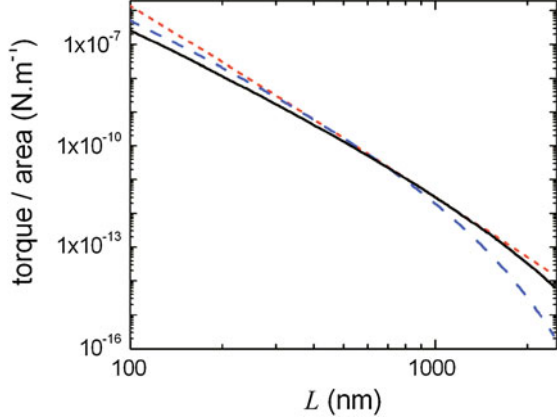
(4.19) and the evaluation of scattering properties mixing different wavevectors and polarizations.

In the following we briefly discuss the Casimir interaction energy in a typical device made of two nanostructured surfaces of intrinsic silicon, such as shown in Fig. 4.6.

To model the material properties of intrinsic silicon, we use a Drude–Lorentz model for which the dielectric function is well approximated by [142]

$$\varepsilon(i\xi) = \varepsilon_\infty + \frac{(\varepsilon_0 - \varepsilon_\infty)\xi_0^2}{\xi^2 + \xi_0^2}, \tag{4.29}$$

with $\varepsilon_0 \approx 11.87$ the value of the dielectric function at zero frequency, $\varepsilon_\infty \approx 1.035$ the high frequency limit of the dielectric function and $\omega_0 = i\xi_0 \approx 4.34\,\text{eV}$. Calculated with the proximity force approximation, the Casimir force between the two gratings is given by the geometric sum of two contributions corresponding to the Casimir force between two plates F_{PP} at distances L and $L - 2h$, which is independent of the corrugation period d.

To assess quantitatively the validity of the PFA, we plot as before the dimensionless quantity

$$\rho = \frac{F}{F_{\text{PFA}}}. \tag{4.30}$$

Fig. 4.7 shows this ratio for two silicon gratings, separated by $L = 250\,\text{nm}$, of height $h = 100\,\text{nm}$ as a function of the corrugation period d with $d_1 = d/2$ [82]. Clearly, the PFA is not a valid approximation except for two limiting cases, that is a vanishing corrugation period $d \to 0$ and a very large corrugation period $d \to \infty$, meaning in either case that the structured surfaces become flat. In between, the exact result for the Casimir force is always smaller than the PFA prediction, meaning that the PFA overestimates the force. This has to be contrasted with calculations for perfect conductors where the PFA always underestimates the real force.

Fig. 4.6 Two surfaces with rectangular gratings of depth h, gap width d and trench width $d - d_1$
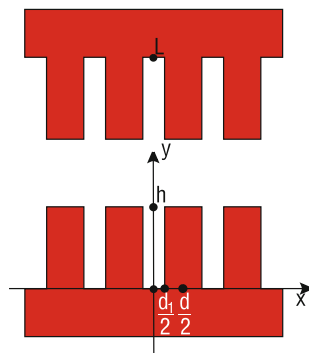
Fig. 4.7 Casimir force normalized by its PFA value for two gratings of intrinsic silicon with amplitude $h = 100$ nm and $d_1 = \frac{d}{2}$ as a function of d at a fixed distance $L = 250$ nm
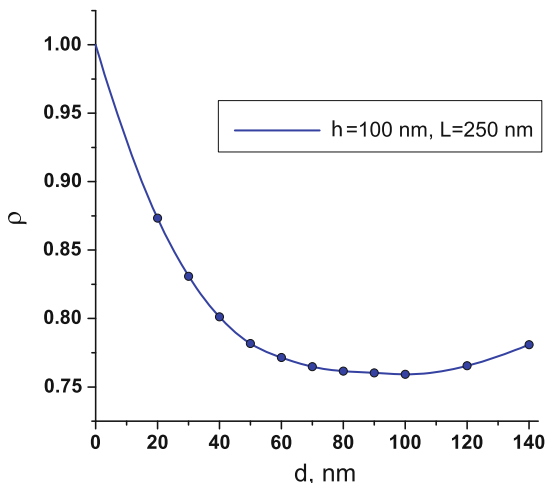
One important parameter to keep in mind is the number of diffraction orders that has to be retained in the calculation in order for the Casimir energy to converge in the numerical calculation. This is illustrated in Fig. 4.8 for two silicon gratings. For the sake of convenience, we plot the Casimir energy normalized by the energy for perfectly reflecting plane mirrors, i.e. the energy reduction factor. The blue curve corresponds to the situation of two gratings of period 400 nm separated by a distance $L = 50$ nm. Clearly around five orders of diffraction are sufficient for the calculation of the Casimir energy in this case. The number of necessary diffraction orders decreases with increasing distance between the gratings. This is illustrated by the red curve where the two aforementioned gratings are now separated by a distance $L = 400$ nm and where the Casimir energy has basically converged to its final value with only one order of diffraction retained. The fast convergence is here due to that fact that oblique diffraction orders are
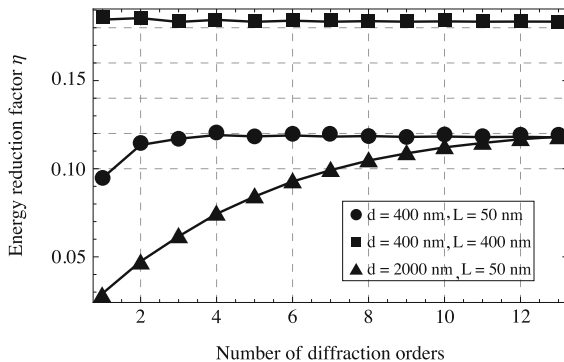
Fig. 4.8 Convergence of the calculated Casimir energy between two gratings as a function of the number of diffraction orders retained in the calculation. Gratings with different periods are plotted as circles and squares (400 nm) and triangles (2 μm). The convergence of the calculations becomes slower when increasing the grating period d or decreasing the separation L

exponentially suppressed with increasing distance [112]. Finally, the greater the period of the grating the more orders of diffractions are needed as shows the curve with triangles where the period of the two gratings is now 2 μm. In this case, the Casimir energy has not yet fully converged to its final value even with as much as 13 orders of diffraction. This can be understood because the momentum transferred by the grating $q = \frac{2\pi}{d}$ is now small so that different orders of diffraction are nearly collinear with the specular one and therefore greatly contribute to the final energy.

If attention is paid to the issue of convergence this calculation method is essentially exact and allows for direct comparisons with experimental results. In a recent experiment, Chan et al. have measured the Casimir force gradient between a gold sphere and a grating of doped silicon [80]. Two samples of silicon gratings have been used. Both have a corrugation depth of 1μm, but different periods of 400 nm and 1μm respectively. The experimental data points of the ratio between the force gradient and its PFA approximation for both samples have been kindly provided by Ho Bun Chan and are plotted in Fig. 4.9. Experimentally the trench arrays are created with duty cycle close to but not exactly equal to 50%. This results in a filling factor p which gives the top part of the grating with respect to the period. See also the chapter by Capasso et al. in this volume for further details of this experiment.

Concerning the calculation we model the optical properties of silicon by the dielectric function (4.29). We have also taken into account the doping of the silicon by adding a Drude part to this dielectric function, but this has not led to noticeable changes for the Casimir interaction in the distance range up to 500 nm which has been explored in the experiment. To model the optical properties of gold we have used available optical data, extrapolated at low frequencies by a Drude model $\varepsilon(i\xi) = \frac{\omega_p^2}{\xi(\xi+\gamma)}$ with $\omega_p = 9\,\text{eV}$ and $\gamma = 35\,\text{meV}$. The method is described in detail in [36]. The calculations were run up to $N = 3$ diffraction orders, after which
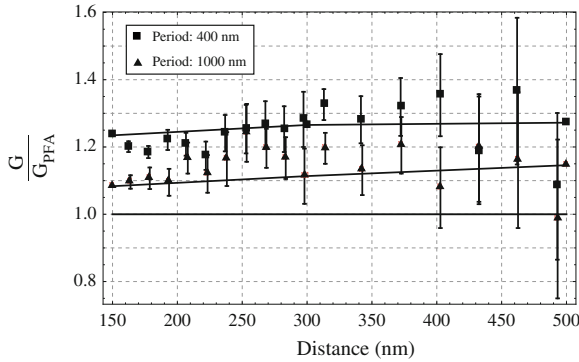
Fig. 4.9 Comparisons between experimental measurements and exact calculations for the Casimir force gradient between a gold sphere and two types of silicon gratings. Squares and circles correspond to data points provided by Ho Bun Chan for a grating period of 400 nm and 1 µm respectively. The solid curves are calculated data obtained using the scattering approach for the corresponding experimental parameters

Fig. 4.10 Same plot as Fig. 4.9, but with corrected filling factors
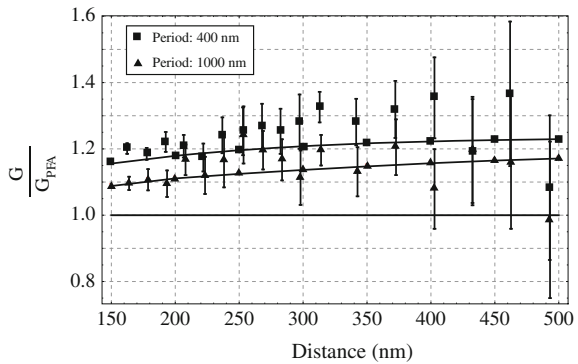
the result for the Casimir energy was found to have converged. The result of our calculation for the filling factors such as originally given in [80] is shown in Fig. 4.9 as the solid green and red curves for the 400 nm ($p = 0.51$) and 1 µm ($p = 0.48$) samples respectively. The theoretical predictions and the experimental data points are in excellent agreement. In particular, due to a new improved numerical code the agreement is better than the one presented in [82].

After submitting this paper we have been informed by Chan et al. that the filling factors in [80] were erroneously interchanged. The correct filling factors are: $p = 0.48$ for the 400 nm grating and $p = 0.51$ for the 1 µm grating. In Fig. 4.10 we show the same calculations as before but with the new filling factors. The agreement between experimental and theoretical data points is slightly degraded for the 400 nm grating, but the overall agreement remains very good.

4.4.3 Exact Calculations in the Plane-sphere Geometry

The plane-sphere geometry is the configuration in which the most precise Casimir force measurements are currently performed [73]. The Casimir interaction in this geometry can also be calculated in a formally exact manner using the general scattering formula (4.19). Such calculations have first been performed for perfectly reflecting mirrors [68, 69] where it was found that the Casimir energy was smaller than expected from the PFA and, furthermore, that the result for electromagnetic fields was departing from PFA more rapidly than was expected from previously existing scalar calculations [65, 66]. It is only very recently that the same calculations have been performed for the more realistic case of metallic mirrors at zero temperature [70] and at arbitrary temperature [71, 72] where both the lossless plasma model dielectric function and the lossy Drude dielectric function have been studied. We will sketch the method in the following.

The set-up of a sphere of radius R above a flat plate is schematically presented in Fig. 4.11. We denote respectively L and $\mathcal{L} \equiv L + R$ the closest approach distance and the center-to-plate distance. In this configuration, the general expression of the Casimir free energy at temperature T may be written as

$$\mathcal{F} = k_\mathrm{B} T \sum_m {}' \mathrm{Tr} \ln D(i\xi_m), \quad D \equiv 1 - R_\mathrm{S} e^{-K\mathcal{L}} R_\mathrm{P} e^{-K\mathcal{L}}. \tag{4.31}$$

The expression contains the reflection operators of the sphere R_S and the plate R_P which are evaluated with reference points placed at the sphere center and at its projection on the plane of the plate. They are sandwiched in between operators $e^{-K\mathcal{L}}$ describing the propagation between the two reference points.

The upper expression is conveniently written through a decomposition on suitable plane-wave and multipole basis [70]; R_P is thus expressed in terms of the Fresnel reflection coefficients r_p with $p = \mathrm{TE}$ and TM for the two electromagnetic polarizations, while R_S contains the Mie coefficients a_ℓ, b_ℓ for respectively electric and magnetic multipoles at order $\ell = 1, 2, \dots$. Due to rotational symmetry around the z-axis, each eigenvalue of the angular momentum m gives a separate contribution to the Casimir free energy $\mathcal{F}^{(m)}$, obtained through the same formula as (4.31). The scattering formula is obtained by writing also transformation formulas from the plane waves basis to the spherical waves basis and conversely.

The result takes the form of a multipolar expansion with spherical waves labeled by ℓ and m ($|m| \leq \ell$). It can be considered as an "exact" multipolar series of the Casimir free energy. Of course, the numerical computations of this series can only be done after truncating the vector space at some maximum value ℓ_max of the orbital index ℓ.

The effect of this truncation is represented on Fig. 4.12 where the Casimir energy in the plane-sphere geometry divided by its PFA estimation

$$\rho_E = \frac{E}{E^{\mathrm{PFA}}} \tag{4.32}$$

Fig. 4.11 The geometry of a sphere of radius R and a plate at distance L; the center-to-plate distance is $\mathcal{L} \equiv L + R$
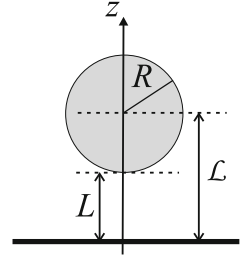
is plotted for various values of $\ell_{\max}$, in the special case of perfect mirrors in vacuum ($T = 0$). The figure shows that as expected the numerical results are more and more accurate when $\ell_{\max}$ is increased. More precisely the accuracy is significantly degraded when the ratio L/R goes below a minimal value inversely proportional to $\ell_{\max}$

$$x \equiv \frac{L}{R} > x_{\min}, \quad x_{\min} \propto \frac{1}{\ell_{\max}}. \tag{4.33}$$

To illustrate the effect of the truncation, one may say that the accuracy is degraded by typically more than 0.1% when $x < 0.05$ for a value of $\ell_{\max} = 85$. For small values of x, which corresponds to the most precise current experiments, it may be possible to obtain information through an extrapolation of the numerical results. As an example, the dashed line on Fig. 4.12 shows the result of a third degree polynomial fit using accurate numerical evaluations.

As a further step, we show now on Fig. 4.13 the results corresponding to perfect and plasma mirrors, still at zero temperature [70]. We have derived the Casimir energy (4.31) to obtain expressions for the force F and force gradient G, and then formed the ratios of the plane-sphere exact results to the PFA expectations F^{PFA} and G^{PFA} respectively

$$\rho_F = \frac{F}{F^{\text{PFA}}}, \quad \rho_G = \frac{G}{G^{\text{PFA}}}. \tag{4.34}$$

Using these theoretical evaluations, it is now possible to extract information of interest for a comparison with the experimental study of the PFA in the plane-sphere geometry [73]. In this experiment, the force gradient has been measured for various radii of the sphere and no deviation of the PFA was observed. The authors expressed their result as a constraint on the slope at origin β_G of the function $\rho_G(x)$

$$\rho_G(x) = 1 + \beta_G x + O(x^2), \quad |\beta_G| < 0.4. \tag{4.35}$$

Reasoning along the same lines, we have interpolated our theoretical evaluation of ρ_G at low values of $x = L/R$ [70]. Surprisingly the slope obtained for perfect reflectors was found to lie outside the experimental bound of [73]

$$\beta_G^{\text{perf}} \sim -0.48. \tag{4.36}$$

Fig. 4.12 *Upper graph*: the ratio $\rho_E = E/E^{\mathrm{PFA}}$ of the plane-sphere Casimir energy to its PFA estimation is plotted as a function of $\ell_{\max}$ for different values of $L/R = 0.05, 0.1, 0.2$. *Lower graph*: same ratio ρ_E plotted as a function of L/R for different values of $\ell_{\max} = 20, 40, 80$
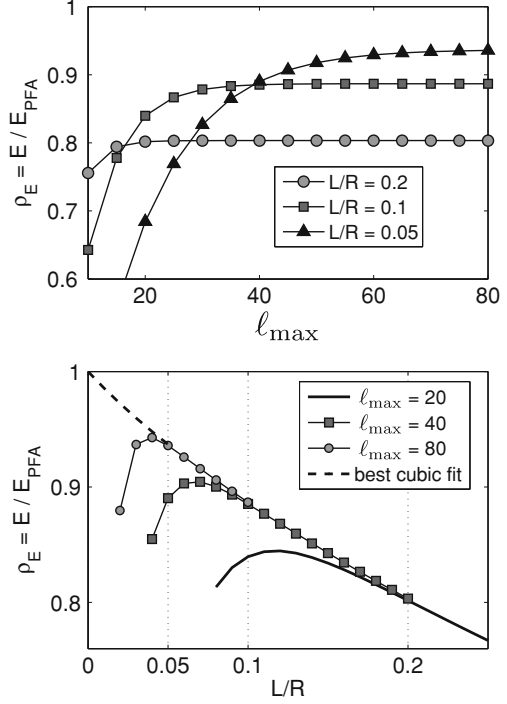
Fig. 4.13 Variation of ρ_G as a function of L/R, for a nanosphere of radius $R = 100$ nm; the solid line corresponds to gold-covered plates ($\lambda_P = 136$ nm) and the dashed line to perfect reflectors. The decrease at low values of L/R represents a numerical inaccuracy due to the limited value of $\ell_{\max}$ (4.24 in this calculation [69])
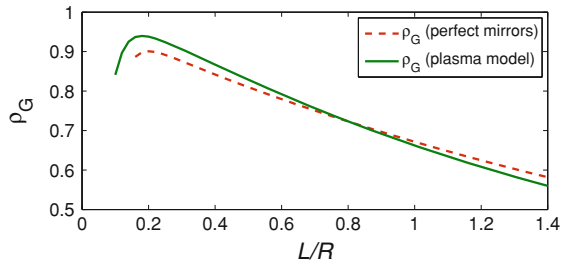

The consistency with this bound is however recovered for the calculations done for plasma mirrors

$$\beta_G^{\mathrm{plas}} \sim -0.21. \tag{4.37}$$

As a last example of application, we now discuss the effect of a non-zero temperature. To this end we evaluate (4.31) at ambient temperature ($T = 300$ K).

Fig. 4.14 Thermal Casimir
force at $T = 300$ K divided
by the zero temperature force,
computed between perfectly
reflecting sphere and plane
(*upper graph*), and between
Drude metals (*lower graph*),
plotted for $\lambda_P = 136$ nm,
$\lambda_\gamma/\lambda_P = 250$. The solid lines
from bottom to top
correspond to increasing
values of sphere radii. The
dotted curve in the upper
graph is the analytical
asymptotic expression in the
$L \gg R$ limit. The PFA
expressions are given by the
dashed curves
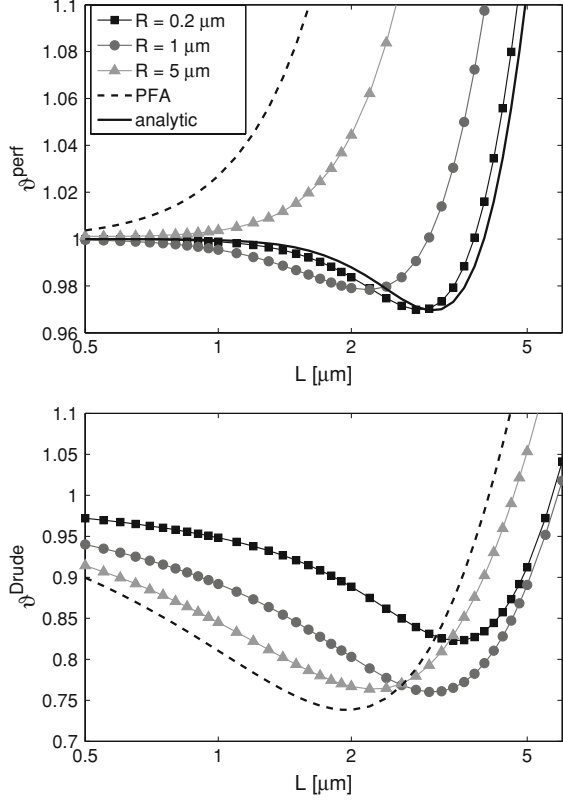
The results of the numerical computations are shown on Fig. 4.14, for the limiting
case of perfect reflection (left) and for Drude metals (right) evaluated for $\lambda_P = 136$ nm, $\lambda_\gamma/\lambda_P = 250$ (values corresponding to gold). We have calculated the
Casimir force F^{perf} and F^{Drud} between the plane and the sphere at ambient tem-
perature and then plotted the corresponding ratios $\vartheta^{\mathrm{perf}}$ and $\vartheta^{\mathrm{Drud}}$ of this force to a
reference force corresponding to zero temperature

$$
\begin{aligned}
F^{\mathrm{perf}}(L, T) &\equiv -\frac{\partial \mathcal{F}^{\mathrm{perf}}}{\partial L}, \quad \vartheta^{\mathrm{perf}} \equiv \frac{F^{\mathrm{perf}}(L, T)}{F^{\mathrm{perf}}(L, 0)}, \\
F^{\mathrm{Drud}}(L, T) &\equiv -\frac{\partial \mathcal{F}^{\mathrm{Drud}}}{\partial L}, \quad \vartheta^{\mathrm{Drud}} \equiv \frac{F^{\mathrm{Drud}}(L, T)}{F^{\mathrm{Drud}}(L, 0)}.
\end{aligned}
\tag{4.38}
$$

The various solid curves are drawn for different sphere radii R as a function of
the separation L; the dashed curves on Fig. 4.14 represent the quantities $\vartheta^{\mathrm{perf}}_{\mathrm{PFA}}$ and
$\vartheta^{\mathrm{Drud}}_{\mathrm{PFA}}$ obtained from (4.38) by using the PFA; the dotted curve in the upper graph is
an analytical asymptotic expression discussed below. We do not show the corre-
sponding plots for plasma mirrors as they are very similar to the perfect mirror
case.

The comparison of $\vartheta^{\mathrm{perf}}$ and $\vartheta^{\mathrm{Drud}}$ reveals surprising features, which could not be expected from an analysis in the parallel-plate geometry. First both ratios ϑ start from unity at small distances $L/R \to 0$. For R small enough, the ratios then decrease below unity with increasing distance, reach a radius-dependent minimum and then increase again at very large distances. This behavior entails that the Casimir force is smaller at $T{=}300$ K than at $T = 0$, implying a repulsive contribution from thermal fluctuations. The dotted-dashed PFA curve in the upper graph of Fig. 4.14 representing $\vartheta^{\mathrm{perf}}_{\mathrm{PFA}}$ is always larger than unity, excluding such a repulsive contribution from thermal fluctuations in the plane-plane geometry.

A second important feature showing up in Fig. 4.14 is that the PFA expression always overestimates the effect of temperature on the force between perfect (and plasma) mirrors. However between Drude metals, the PFA underestimates this effect at small distances and overestimates it at large distances, the overestimation being however smaller than for perfect mirrors. These results clearly indicate that there is a strong correlation between the effects of plane-sphere geometry, temperature and dissipation.

The calculation of the Casimir free energy may be done analytically for small frequencies corresponding to large plane-sphere separations

$$\mathcal{F}^{\mathrm{perf}}_{\ell=1} = -\frac{3\hbar c R^3}{4\lambda_{\mathrm{T}} L^3}\phi(v), \quad v \equiv \frac{2\pi L}{\lambda_{\mathrm{T}}},$$

$$\phi(v) \equiv \frac{v^2 \cosh v + v \sinh v + \cosh v \sinh^2 v}{2\sinh^3 v}. \tag{4.39}$$

This simple expression is a good approximation, as proven by the fact that the full expression of $\vartheta^{\mathrm{perf}}$ tends indeed asymptotically to this simple form for small radii $R \ll L$ (dotted line on upper graph of Fig. 4.14). One can also derive from this expression interesting information about the behavior of the Casimir entropy

$$S^{\mathrm{perf}}_{\ell=1} = -\frac{\partial \mathcal{F}^{\mathrm{perf}}_{\ell=1}}{\partial T} = \frac{3k_{\mathrm{B}}R^3}{4L^4}(\phi(v) + v\phi'(v)). \tag{4.40}$$

This expression takes on negative values for $v \lesssim 1.5$, that is $L \lesssim 1.8\,\mu\mathrm{m}$ at $T = 300$ K, which is in agreement with the behavior observed in the upper graph of Fig. 4.14: in most cases $\vartheta^{\mathrm{perf}}$ decreases below unity as the distance increases, reaches a minimum and then increases again at long distances. As long as R is not too large, the thermal photons provide a repulsive contribution over a distance range that gets wider as R decreases, to become $L \lesssim \lambda_T/2$ for very small spheres.

We finally will compare the predictions of the dissipationless plasma model and the dissipative Drude model for the thermal Casimir interaction in the plane-sphere geometry. The difference will become particularly clear in the high temperature limit $\mathcal{L} \gg \lambda_T$ where one only needs to take the first Matsubara frequency $\xi_0 = 0$ when computing the Casimir free energy. In the low frequency limit, the Fresnel coefficients (4.16) for the plates are given by $r_{\mathrm{TE}} \approx -r_{\mathrm{TM}} \approx -1$ for the

Fig. 4.15 Ratio of thermal Casimir force at T=300 K calculated with the plasma model and the Drude model, as a function of surface separation L for different radii of the sphere. The solid curves from bottom to top correspond to increasing values of sphere radii. The dashed curve is the PFA prediction
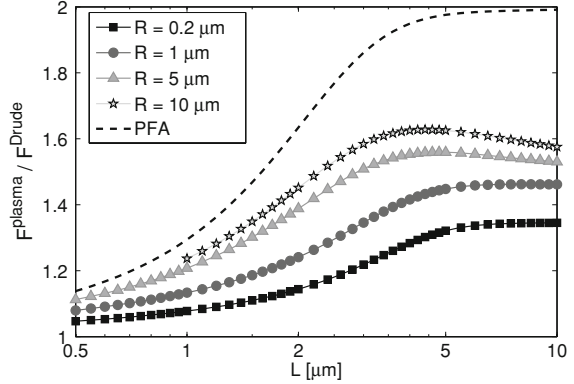
plasma model. The Mie coefficients are easily evaluated [71, 72] and give the following approximation for the Casimir force within the plasma model

$$\mathcal{F}^{\text{plas}} \approx -\frac{3\hbar c R^3}{8\lambda_T \mathcal{L}^3}\left(1 + \frac{1}{\alpha^2} - \frac{\coth \alpha}{\alpha}\right) \mathcal{L} \gg \lambda_T, R, \lambda_P, \alpha \equiv \frac{2\pi R}{\lambda_P}.$$

This result reproduces, as a particular case, the perfectly-reflecting limit when $\lambda_P \ll R$.

For the Drude model, the TE Fresnel reflection coefficient has the well-known low-frequency limit $r_{\text{TE}} \rightarrow 0$, whereas the TM coefficient behaves as in the plasma model: $r_{\text{TM}} \approx 1$. The low-frequency expansion of the Mie coefficients are also quite different from the plasma case and can be found in [71, 72]. The resulting high-temperature large-distance limit for the free energy is

$$\mathcal{F}^{\text{Drud}} \approx -\frac{\hbar c R^3}{4\lambda_T \mathcal{L}^3} \quad , \quad \mathcal{L} \gg \lambda_T, R. \tag{4.41}$$

This remarkable result does not depend on the length scales λ_P and λ_γ characterizing the material response, whereas the corresponding plasma result (4.41) clearly depends on λ_P. One can show that this is always the case in the high-temperature limit $\lambda_T \ll \mathcal{L}$.

In the case of the Drude model with a non-vanishing relaxation frequency the free energy for the Drude model turns out to be 2/3 of the expression for perfect mirrors whereas this ratio is 1/2 in the plane-plane geometry. The latter result is explained by the fact that the TE reflection coefficient vanishes at zero frequency so that only the TM modes contribute [42, 45]. The change of the ratio 1/2–2/3 in the plane-sphere geometry has to be attributed to the redistribution of the TE and TM contributions into electric and magnetic spherical eigenmodes. The change is illustrated in Fig. 4.15, where we have plotted the ratio of the thermal Casimir force F^{plas} calculated with the plasma model to the one F^{Drud} obtained with the Drude model. Again, the plots correspond to $\lambda_P = 136$ nm and $\lambda_\gamma/\lambda_P = 250$.

The results of our calculations are shown by the solid curves with the sphere radius increasing from bottom to top. The ratio $F^{\text{plas}}/F^{\text{Drud}}$ varies in the plane-sphere geometry as a function of the sphere radius, clearly demonstrating the strong interplay between the effects of temperature, dissipation and geometry. For large spheres ($R \gg \lambda_{\text{P}}$), the ratio converges to the value 3/2, whereas it remains smaller for small spheres (down to 1.2 for $R \sim 100$ nm). The dashed curve gives the variation of the same ratio as calculated within the PFA which leads to a factor of 2 in the limits of large distances or high temperatures, corresponding to the prediction in the parallel-plates geometry. This factor of 2 deduced within the PFA is never approached within the calculations performed in the plane-sphere geometry.

4.5 Conclusion

In this paper we have reviewed the quantum and thermal Casimir interaction between parallel plates, corrugated surfaces and plane and spherical mirrors. To perform our calculations we have extensively used the scattering approach where the objects are characterized by scattering matrices. We have compared our results with predictions obtained within the PFA. When taking the diffraction of the electromagnetic field correctly into account, surprising features appear especially for the thermal Casimir force in the plane-sphere geometry, where the exact results differ substantially from predictions within the PFA. While open problems are still waiting to be tackled, the whole set of presented results clearly illustrates the usefulness and practicality of the scattering approach in Casimir physics.

References

1. Casimir, H.B.G.: Proc. K. Ned. Akad. Wet. **51**, 793 (1948)
2. Milonni, P.W.: The Quantum Vacuum. Academic Press, London (1994)
3. Lamoreaux, S.K.: Resource letter CF-1: Casimir force. Am. J. Phys. **67**, 850 (1999)
4. Reynaud, S., Lambrecht, A., Genet, C., Jaekel, M.T.: Quantum vacuum fluctuations. C. R. Acad. Sci. Paris **IV-2**, 1287 (2001)
5. Bordag, M., Mohideen, U., Mostepanenko, V.M.: New developments in the Casimir effect. Phys. Rep. **353**, 1 (2001)
6. Milton, K.A.: The Casimir effect: recent controversies and progress. J. Phys. A **37**, R209 (2004)
7. Decca, R.S., López, D., Fischbach, E., Klimchitskaya, G.L., Krause, D.E., Mostepanenko, V.M.: Precise comparison of theory and new experiment for the Casimir force leads to

stronger constraints on thermal quantum effects and long-range interactions. Annals Phys. **318**, 37 (2005)

8. Lambrecht, A., Maia Neto, P.A., Reynaud, S.: The Casimir effect within scattering theory. New J. Phys. **8**, 243 (2006)

9. Jaekel, M.T., Reynaud, S.: Movement and fluctuations of the vacuum. Rep. prog. phys. **60**, 863 (1997)

10. Elizalde, E.: Quantum vacuum fluctuations and the cosmological constant. J Phys A **40**, 6647 (2007)

11. Jaekel M.T., and Reynaud S.: In Proceeding of the Orleans School on Mass (2009)

12. Fischbach, E., Talmadge, C.: The Search for Non Newtonian Gravity. AIP Press/Springer, Berlin (1998)

13. Adelberger, E.G., Heckel, B.R., Nelson, A.E.: Tests of the gravitational inverse-square law. Ann. Rev. Nucl. Part. Sci. **53**, 77 (2009)

14. Kapner, D.J., Cook, T.S., Adelberger, E.G., Gundlach, J.H., Heckel, B.R., Hoyle, C.D., Swanson, H.E.: Tests of the gravitational inverse-square law below the dark-energy length scale. Phys. Rev. Lett. **98**, 021101 (2007)

15. Lambrecht A., and Reynaud S.: Poincaré Seminar on Vacuum Energy and Renormalization **1**, 107 (2002) [arXiv quant-ph/0302073]

16. Onofrio, R.: Casimir forces and non-Newtonian gravitation. New J. Phys. **8**, 237 (2006)

17. Decca, R.S., López, D., Fischbach, E., Klimchitskaya, G.L., Krause, D.E., Mostepanenko, V.M.: Novel constraints on light elementary particles and extra-dimensional physics from the Casimir effect. Eur. Phys. J. C **51**, 963 (2007)

18. Lepoutre, S., Jelassi, H., Lonij, V.P.A., Trenec, G., Buchner, M., Cronin, A.D., Vigue, J.: Dispersive atom interferometry phase shifts due to atom-surface interactions. Europhys. Lett. **88**, 20002 (2009)

19. Nesvizhevsky, V.V., Pignol, G., Protasov, K.V.: Neutron scattering and extra-short-range interactions. Phys. Rev. D **77**, 034020 (2008)

20. Parsegian, V.A.: Van der Waals Forces: a Handbook for Biologists, Chemists, Engineers, and Physicists. Cambridge University Press, Cambridge (2006)

21. Sparnaay M.J.: In Physics in the Making. Eds Sarlemijn A., and Sparnaay M.J., North-Holland (1989)

22. Lamoreaux, S.K.L.: Demonstration of the casimir force in the 0.6 to 6 mu m range. Phys. Rev. Lett. **78**, 5 (1997)

23. Mohideen, U., Roy, A.: Precision measurement of the Casimir force from 0.1 to 0.9 mu m. Phys. Rev. Lett. **81**, 4549 (1998)

24. Harris, B.W., Chen, F., Mohideen, U.: Precision measurement of the Casimir force using gold surfaces. Phys. Rev. A **62**, 052109 (2000)

25. Ederth, T.: Template-stripped gold surfaces with 0.4 nm rms roughness suitable for force measurements: Application to the Casimir force in the 20–100 nm range. Phys. Rev. A **62**, 062104 (2000)

26. Bressi, G., Carugno, G., Onofrio, R., Ruoso, G.: Measurement of the Casimir force between parallel metallic surfaces. Phys. Rev. Lett **88**, 041804 (2002)

27. Decca, R.S., López, D., Fischbach, E., Krause, D.E.: Measurement of the Casimir force between dissimilar metals. Phys. Rev. Lett. **91**, 050402 (2003)

28. Chen, F., Klimchitskaya, G.L., Mohideen, U., Mostepananko, V.M.: Theory confronts experiment in the Casimir force measurements: Quantification of errors and precision. Phys. Rev. A **69**, 022117 (2004)

29. Decca, R.S., López, D., Fischbach, E., Klimchitskaya, G.L., Krause, D.E., Mostepanenko, V.M.: Tests of new physics from precise measurements of the Casimir pressure between two gold-coated plates. Phys. Rev. D **75**, 077101 (2007)

30. Munday, J.N., Capasso, F.: Precision measurement of the Casimir-Lifshitz force in a fluid. Phys. Rev. A **75**, 060102(R) (2007)

31. van Zwol, P.J., Palasantzas, G., De Hosson, J.T.M.: Influence of random roughness on the Casimir force at small separations. Phys. Rev. B **77**, 075412 (2008)

32. Munday, J.N., Capasso, F., Parsegian, V.A.: Measured long-range repulsive Casimir-Lifshitz forces. Nature **457**, 170 (2009)
33. Jourdan, G., Lambrecht, A., Comin, F., Chevrier, J.: Quantitative non-contact dynamic Casimir force measurements. Europhys. Lett. **85**, 31001 (2009)
34. Masuda, M., Sasaki, M.: Limits on nonstandard forces in the submicrometer range. Phys. Rev. Lett. **102**, 171101 (2009)
35. de Man, S., Heeck, K., Wijngaarden, R.J., Iannuzzi, D.: Halving the casimir force with conductive oxides. Phys. Rev. Lett. **103**, 040402 (2009)
36. Lambrecht, A., Reynaud, S.: Casimir force between metallic mirrors. Euro. Phys. J. D **8**, 309 (2000)
37. Svetovoy, V.B., van Zwol, P.J., Palasantzas, G., De Hosson, J.T.M.: Optical properties of gold films and the Casimir force. Phys. Rev. B **77**, 035439 (2008)
38. Mehra, J.: Temperature correction to the casimir effect. Physica **37**, 145 (1967)
39. Brown, L.S., Maclay, G.J.: Vacuum stress between conducting plates: an image solution. Phys. Rev. **184**, 1272 (1969)
40. Schwinger, J., de Raad, L.L., Milton, K.A.: Casimir effect in dielectrics. Ann. Phys. **115**, 1 (1978)
41. Genet, C., Lambrecht, A., Reynaud, S.: Temperature dependence of the Casimir effect between metallic mirrors. Phys. Rev. A **62**, 012110 (2000)
42. Boström, M., Sernelius, B.E.: Thermal effects on the Casimir force in the 0.1-5 mu m range. Phys. Rev. Lett. **84**, 4757 (2000)
43. Reynaud S., Lambrecht A., and Genet C.: In Quantum Field Theory Under the Influence of External Conditions. Ed. Milton K.A., Rinton Press (2004) [arXiv quant-ph/0312224]
44. Klimchitskaya, G.L., Mostepanenko, V.M.: Experiment and theory in the Casimir effect. Contemp. Phys. **47**, 131 (2006)
45. Brevik, I., Ellingsen, S.E., Milton, K.A.: Thermal corrections to the Casimir effect. New J. Phys. **8**, 236 (2006)
46. Brevik, I., Ellingsen, S.E., Høye, J.S., Milton, K.A.: Analytical and numerical demonstration of how the Drude dispersive model satisfies Nernst's theorem for the Casimir entropy. J. Phys. A **41**, 164017 (2008)
47. Milton, K.A.: Recent developments in the Casimir effect. J. Phys. Conf. Ser. **161**, 012001 (2009)
48. Jancovici, B., Šamaj, L.: Casimir force between two ideal-conductor walls revisited. Europhys. Lett. **72**, 35 (2005)
49. Buenzli, P.R., Martin, P.A.: The Casimir force at high temperature. Europhys. Lett. **72**, 42 (2005)
50. Bimonte, G.: Bohr-van Leeuwen theorem and the thermal Casimir effect for conductors. Phys. Rev. A **79**, 042107 (2009)
51. Bezerra, V.B., Klimchitskaya, G.L., Mostepanenko, V.M.: Correlation of energy and free energy for the thermal casimir force between real metals. Phys. Rev. A **66**, 062112 (2002)
52. Ingold, G.L., Lambrecht, A., Reynaud, S.: Quantum dissipative Brownian motion and the Casimir effect. Phys. Rev. E **80**, 041113 (2009)
53. Deriagin, B.V., Abrikosova, I.I., Lifshitz, E.M.: Quart. Rev. **10**, 295 (1968)
54. Lifshitz, E.M.: The theory of molecular attractive forces between solids. Sov. Phys. JETP **2**, 73 (1956)
55. Dzyaloshinskii, I.E., Lifshitz, E.M., Pitaevskii, L.P.: The general theory of van der Waals forces. Sov. Phys. Uspekhi **4**, 153 (1961)
56. Balian, R., and Duplantier, B.: Electromagnetic waves near perfect conductors. I. Multiple scattering expansions. Distribution of modes. Ann. Phys. NY **104**,300 (1977)
57. Balian, R., and Duplantier, B.: Electromagnetic waves near perfect conductors. II. Casimir effect. Ann. Phys. NY **112**,165 (1978)
58. Balian R.: In Poincaré Seminar 2002 on Vacuum Energy. Eds Duplantier B., and Rivasseau V., Birkhäuser (2003)
59. Balian R., and Duplantier B.: In 15th SIGRAV Conference on General Relativity and Gravitation.[arXiv quant-ph/0408124] (2004)

60. Schaden, M., Spruch, L.: Focusing virtual photons: Casimir energies for some pairs of conductors. Phys. Rev. Lett. **84**, 459 (2000)
61. Jaffe, R.L., Scardicchio, A.: Casimir effect and geometric optics. Phys. Rev. Lett. **92**, 070402 (2004)
62. Schröder, O., Sardicchio, A., Jaffe, R.L.: Casimir energy for a hyperboloid facing a plate in the optical approximation. Phys. Rev. A **72**, 012105 (2005)
63. Reynaud, S., Maia Neto, P.A., Lambrecht, A.: Casimir energy and geometry: beyond the proximity force approximation. J. Phys. A **41**, 164004 (2008)
64. Emig, T., Graham, N., Jaffe, R.L., Kardar, M.: Casimir forces between arbitrary compact objects. Phys. Rev. Lett **99**, 170403 (2007)
65. Bordag, M., Nikolaev, V.: Casimir force for a sphere in front of a plane beyond proximity force approximation. J. Phys. A **41**, 164002 (2008)
66. Wirzba, A.: The Casimir effect as a scattering problem. J. Phys. A **41**, 164003 (2008)
67. Klingmüller, K., Gies, H.: Geothermal Casimir phenomena. J. Phys. A **41**, 164042 (2008)
68. Emig T.: Fluctuation-induced quantum interactions between compact objects and a plane mirror. J. Stat. Mech. Theory Exp. P04007 (2008)
69. Maia Neto, P.A., Lambrecht, A., Reynaud, S.: Casimir energy between a plane and a sphere in electromagnetic vacuum. Phys. Rev. A **78**, 012115 (2008)
70. Canaguier-Durand, A., Maia Neto, P.A., Cavero-Pelaez, I., Lambrecht, A., Reynaud, S.: Casimir interaction between plane and spherical metallic surfaces. Phys. Rev. Lett. **102**, 230404 (2009)
71. Canaguier-Durand, A., MaiaNeto P., A., Lambrecht, A., Reynaud, S.: Thermal Casimir effect in the plane-sphere geometry. Phys. Rev. Lett. **104**, 040403 (2010)
72. Canaguier-Durand A., Maia Neto P.A., Lambrecht A., and Reynaud S. Thermal Casimir effect for Drude metals in the plane-sphere geometry. submitted [arXiv:1005.4294] (2010)
73. Krause, D.E., Decca, R.S., López, D., Fischbacoh, E.: Experimental investigation of the Casimir force beyond the proximity-force approximation. Phys. Rev. Lett. **98**, 050403 (2007)
74. Chen, F., Mohideen, U., Klimchitskaya, G.L., and Mostepanenko, V.M.: Demonstration of the lateral Casimir force. Phys. Rev. Lett. **88**,101801 (2002)
75. Chen, F., Mohideen, U., Klimchitskaya, G.L., and Mostepanenko, V.M.: Demonstration of the lateral Casimir force. Phys. Rev. Lett. **66**, 032113 (2002)
76. Büscher, R., Emig, T.: Geometry and spectrum of Casimir forces. Phys. Rev. Lett. **94**, 133901 (2005)
77. Rodrigues, R.B., Maia Neto, P.A., Lambrecht, A., and Reynaud, S.:Lateral casimir force beyond the proximity-force approximation. Phys. Rev. Lett. **96**,100402 (2006)
78. Rodrigues, R.B., Maia Neto, P.A., Lambrecht, A., and Reynaud, S.:Lateral casimir force beyond the proximity-force approximation. Reply. Phys. Rev. Lett. **98**,068902 (2007)
79. Rodrigues, R.B., Maia Neto, P.A., Lambrecht, A., Reynaud, S.: Lateral Casimir force beyond the proximity force approximation: A nontrivial interplay between geometry and quantum vacuum. Phys. Rev. A **75**, 062108 (2007)
80. Chan, H.B., Bao, Y., Zou, J., Cirelli, R.A., Klemens, F., Mansfield, W.M., Pai, C.S.: Measurement of the Casimir force between a gold sphere and a silicon surface with nanoscale trench arrays. Phys. Rev. Lett. **101**, 030401 (2008)
81. Chiu, H.C., Klimchitskaya, G.L., Marachevsky, V.N., Mostepanenko, V.M., Mohideen, U.: Demonstration of the asymmetric lateral Casimir force between corrugated surfaces in the nonadditive regime. Phys. Rev. B **80**, 121402 (2009)
82. Lambrecht, A., Marachevsky, V.N.: Casimir interaction of dielectric gratings. Phys. Rev. Lett. **101**, 160403 (2008)
83. Lambrecht, A.: Nanotechnology - Shaping the void. Nature **454**, 836 (2008)
84. Jaekel M.T., and Reynaud S.: Casimir force between partially transmitting mirrors. J. Physique I-1 1395 (1991) [arXiv quant-ph/0101067]
85. Genet, C., Lambrecht, A., Reynaud, S.: Casimir force and the quantum theory of lossy optical cavities. Phys. Rev. A **67**, 043811 (2003)

86. Milton, K.A., Wagner, J.: Multiple scattering methods in Casimir calculations. J. Phys. A **41**, 155402 (2008)
87. Bulgac, A., Magierski, P., Wirzba, A.: Scalar Casimir effect between Dirichlet spheres or a plate and a sphere. Phys. Rev. D **73**, 025007 (2006)
88. Bordag, M.: Casimir effect for a sphere and a cylinder in front of a plane and corrections to the proximity force theorem. Phys. Rev. D **73**, 125018 (2006)
89. Kenneth, O., and Klich, I.: Opposites attract: A theorem about the Casimir force. Phys. Rev. Lett. **97**,160401 (2006)
90. Kenneth, O., and Klich, I.: Opposites attract: A theorem about the Casimir force. Phys. Rev. B **78**,014103 (2008)
91. Emig, T., Jaffe R., L.: Casimir forces between arbitrary compact objects. J. Phys. A **41**, 164001 (2008)
92. Rahi, S.J., Emig, T., Graham, N., Jaffe, R.L., Kardar, M.: Scattering theory approach to electrodynamic Casimir forces. Phys. Rev. D **80**, 085021 (2009)
93. Langfeld, K., Moyaerts, L., Gies, H.: Casimir effect on the worldline. J. High En. Phys. **0306**, 018 (2003)
94. Gies, H., Klingmüller, K.: Casimir effect for curved geometries: Proximity-force-approximation validity limits. Phys. Rev. Lett. **96**, 220401 (2006)
95. Emig, T., Jaffe, R.L., Kardar, M., Scardicchio, A.: Casimir interaction between a plate and a cylinder. Phys. Rev. Lett. **96**, 080403 (2006)
96. Dalvit, D.A.R., Lombardo, F.C., Mazzitelli, F.D., Onofrio, R.: Exact Casimir interaction between eccentric cylinders. Phys. Rev. A **74**, 020101 (2006)
97. Mazzitelli, F.C., Dalvit, D.A.R., Lombardo, F.C.: Exact zero-point interaction energy between cylinders. New J. Phys. **8**, 240 (2006)
98. Rodriguez, A., Ibanescu, M., Iannuzzi, D., Capasso, F., Joannopoulos, J.D., Johnson, S.G.: Computation and visualization of Casimir forces in arbitrary geometries: Nonmonotonic lateral-wall forces and the failure of proximity-force approximations. Phys. Rev. Lett. **99**, 080401 (2007)
99. Döbrich B., DeKieviet M., and Gies H.: Nonpertubative access to Casimir-Polder forces. arXiv:0910.5889 (2009)
100. Bordag M., and Nikolaev V.: First analytic correction beyond PFA for the electromagnetic field in sphere-plane geometry. arXiv:0911.0146 (2009)
101. Gies H., and Weber A.: Geometry-temperature interplay in the Casimir effect. arXiv:0912.0125 (2009)
102. Bordag M., and Pirozhenko I.: Vacuum energy between a sphere and a plane at finite temperature. arXiv:0912.4047 (2010)
103. Emig T.: Casimir physics: geometry, shape and material. arXiv:1003.0192 (2010)
104. Zandi R., Emig T., and Mohideen U.: Quantum and thermal Casimir interaction between a sphere and a plate: Comparison of Drude and plasma models. arXiv:1003.0068 (2010)
105. Weber A., and Gies H.: Non-monotonic thermal Casimir force from geometry-temperature interplay. arXiv:1003.0430 (2010)
106. Weber A., and Gies H.: Geothermal Casimir phenomena for the sphere-plane and cylinder-plane configurations. arXiv:1003.3420 (2010)
107. Maia Neto, P.A., Lambrecht, A., Reynaud, S.: Roughness correction to the Casimir force: Beyond the proximity force approximation. Europhys. Lett. **69**, 924 (2005)
108. Maia Neto, P.A., Lambrecht, A., Reynaud, S.: Casimir effect with rough metallic mirrors. Phys. Rev. A **72**, 012115 (2005)
109. Rodrigues, R.B., Maia Neto, P.A., Lambrecht, A., Reynaud, S.: Vacuum-induced torque between corrugated metallic plates. Europhys. Lett. **76**, 822 (2006)
110. Rodrigues, R.B., Maia Neto, P.A., Lambrecht, A., Reynaud, S.: Phys. Rev. Lett. **100**, 040405 (2008)
111. Dalvit, D.A.R., Maia Neto, P.A., Lambrecht, A., Reynaud, S.: Probing quantum-vacuum geometrical effects with cold atoms. Phys. Rev. Lett. **100**, 040405 (2008)

112. Messina, R., Dalvit, D.A.R., Maia Neto, P.A., Lambrecht, A., Reynaud, S.: Scattering approach to dispersive atom-surface interactions. Phys. Rev. A **80**, 022119 (2009)
113. Johannson, P., Apell, P.: Geometry effects on the van der Waals force in atomic force microscopy. Phys Rev. B **56**, 4159 (1997)
114. Noguez, C., Roman-Velazquez, C.E., Esquivel-Sirvent, R., Villarreal, C.: High-multipolar effects on the Casimir force: The non-retarded limit. Europhys. Lett. **67**, 191 (2004)
115. Feinberg, G., Sucher, J.: General theory of the van der Waals interactions: A model-independent approach. Phys Rev. A **2**, 2395 (1970)
116. Power, E.A., Thirunamachandran, T.: Zero-point energy differences and many-body dispersion forces. Phys Rev. A **50**, 3929 (1994)
117. Jaekel, M.T., Reynaud, S.: Fluctuations and dissipation for a mirror in vacuum. Quantum Opt. **4**, 39 (1992)
118. Jaekel, M.T., Reynaud, S.: Motional Casimir force. Journal de Physique I- **2**, 149 (1992)
119. Jaekel, M.T., Reynaud, S.: Causality, stability and passivity for a mirror in vacuum. Phys. Lett. A **167**, 227 (1992)
120. Jaekel, M.T., Reynaud, S.: Friction and inertia for a mirror in a thermal field. Phy. Lett. A **172**, 319 (1993)
121. Jaekel, M.T., Reynaud, S.: Quantum fluctuations of position of a mirror in vacuum. J. Phys. **I-3**, 1 (1993)
122. Jaekel, M.T., and Reynaud. S.: Inertia of Casimir energy. J. Phys I-3,1093 (1993)
123. Jaekel, M.T., Reynaud, S.: Quantum fluctuations of mass for a mirror in vacuum. Phys. Lett. A **180**, 9 (1993)
124. Lambrecht, A., Jaekel, M.T., Reynaud, S.: Motion induced radiation from a vibrating cavity. Phys. Rev. Lett. **77**, 615 (1996)
125. Lambrecht, A., Jaekel M., T., Reynaud, S.: The Casimir force for passive mirrors. Phys. Lett. A **225**, 188 (1997)
126. Pitaevskii, L.P.: Thermal lifshitz force between an atom and a conductor with a small density of carriers. Phys. Rev. Lett. **101**, 163202 (2008)
127. Geyer, B., Klimchitskaya, G.L., Mohideen, U., Mostepanenko, V.M.: Comment on "Contribution of Drifting Carriers to the Casimir-Lifshitz and Casimir-Polder Interactions with Semiconductor Materials". Phys. Rev. Lett. **102**, 189301 (2009)
128. Pitaevskii, L.P.: Phys. Rev. Lett. **102**, 189302 (2009)
129. Dalvit, D.A.R., Lamoreaux, S.K.: Contribution of drifting carriers to the Casimir-Lifshitz and Casimir-Polder interactions with semiconductor materials. Phys. Rev. Lett. **101**, 163203 (2008)
130. Decca, R.S., Fischbach, E., Geyer, B., Klimchitskaya, G.L., Krause, D.E., Lopez, D., Mohideen, U., Mostepanenko, V.M.: Comment on "Contribution of Drifting Carriers to the Casimir-Lifshitz and Casimir-Polder Interactions with Semiconductor Materials". Phys. Rev. Lett. **102**, 189303 (2009)
131. Dalvit, D.A.R., Lamoreaux, S.K.: Phys. Rev. Lett. **102**, 189304 (2009)
132. Svetovoy, V.B.: Application of the Lifshitz theory to poor conductors. Phys. Rev. Lett. **101**, 163603 (2008)
133. Svetovoy, V.B.: Application of the Lifshitz theory to poor conductors. Phys. Rev. Lett. **102**, 219903(E) (2009)
134. Kats, E.I.: JETP **46**, 109 (1977)
135. Barnett, S.M., Jeffers, J., Gatti, A., Loudon, R.: Quantum optics of lossy beam splitters. Phys. Rev. A **57**, 2134 (1998)
136. Dalvit, D.A.R., Lombardo, F.C., Mazzitelli, F.D., Onofrio, R.: Casimir force between eccentric cylinders. EuroPhys. Lett. **67**, 517 (2004)
137. Mazzitelli, F.D., Dalvit, D.A.R., Lombardo, F.C.: Exact zero-point interaction energy between cylinders. New Journal of Physics **8**, 240 (2006)
138. Bordag, M., Nikolaev, V.: The vacuum energy for two cylinders with one increasing in size. J. Phys. A **42**, 415203 (2009)

139. Zaheer S., Rahi J., Emig T., and Jaffe R. L.: Casimir interactions of an object inside a spherical metal shell. arXiv 0908.3270 (2009)
140. Chiu, H.C., Klimchitskaya, G.L., Marachevsky, V.N., Mostepanenko, V.M., Mohideen, U.: Lateral Casimir force between sinusoidally corrugated surfaces: Asymmetric profiles, deviations from the proximity force approximation, and comparison with exact theory. Phys. Rev. B **81**, 115417 (2010)
141. Munday, J., Ianuzzi, D., Barash, Y., Capasso, F.: Torque on birefringent plates induced by quantum fluctuations. Phys. Rev. A **71**, 042102 (2005)
142. Bergström, L.: Hamaker constants of inorganic materials. Adv. in Colloid. and Interf. Sci. **70**, 125 (1997)